—Supplementary Information—

Strategies for Fitting Accurate Machine Learned Inter-atomic Potentials for Solid Electrolytes

Juefan Wang,[†] Abhishek A. Panchal,[†] and Pieremanuele Canepa[*,†,‡]

[†]*Department of Materials Science and Engineering, National University of Singapore, 9 Engineering Drive 1, 117575, Singapore*

[‡]*Department of Chemical and Biomolecular Engineering, National University of Singapore, 4 Engineering Drive 4, 117585, Singapore*

E-mail: pcanepa@nus.edu.sg

Contents

Sec. S1 Inaccuracies of MTP Training and Validation

Table S1: The training and validation Mean Absolute Errors (MAE) on energies per atom (in meV/atom) and forces (in meV/Å) for the fitted Moment Tensor Potentials (MTPs) of argyrodite Li_6PS_5Cl.

	Training MAE		Validation MAE	
	Energy	**Force**	**Energy**	**Force**
	Exchange-correlation functional			
PBE	4.70	50.50	2.07	45.63
PBEsol	4.93	64.26	8.66	75.30
SCAN+rvv10	6.35	56.25	6.50	64.68
optB88	6.26	78.63	7.22	85.18
	Temperature			
High Temperature	8.61	97.44	11.22	122.48
	Simulation time			
Less snapshots	5.98	75.45	15.00	138.38

Table S2: The training and validation MAE on energies per atom (in meV/atom) and forces (in meV/Å) for the fitted MTPs of argyrodite Li_6PS_5Cl containing different types of defects. The functional used is PBEsol.

	Training MAE		Validation MAE	
	Energy	**Force**	**Energy**	**Force**
Li_i	4.93	64.26	8.66	75.30
Cl_s	5.28	61.69	8.62	72.49
S_{Cl}	2.97	52.85	2.38	49.23
V_{Li}	5.06	80.15	4.47	79.37

Table S3: The training and validation MAE on energies per atom (in meV/atom) and forces (in meV/Å) for the fitted MTPs of argyrodite Li_6PS_5I.

	Training MAE		Validation MAE	
	Energy	**Force**	**Energy**	**Force**
	Exchange-correlation functional			
PBE	2.35	37.96	2.38	37.67
PBEsol	4.32	52.15	4.79	53.63
SCAN+rvv10	2.10	37.47	0.62	20.78
OptB88	2.24	40.82	0.82	20.43
	Temperature			
High Temperature	6.08	71.54	1.68	44.64
	Simulation time			
Less snapshots	5.26	65.15	0.95	29.03

Table S4: Training and validation MAE on energies per atom (in meV/atom) and forces (in meV/Å) of the fitted MTPs of α-Na_3PS_4.

	Training MAE		Validation MAE	
	Energy	**Force**	**Energy**	**Force**
	Exchange-correlation functional			
PBE	1.29	32.71	1.52	34.37
PBEsol	1.20	32.01	1.60	32.00
R2SCAN	1.09	30.43	1.30	31.14
OptB88	0.98	28.09	0.94	28.03
	Temperature			
Low Temperature	0.55	22.71	0.30	19.64
	Simulation time			
More snapshots	1.52	41.24	2.61	57.68

Sec. S2 Calculated Lattice Parameters

Table S5: DFT calculated lattice parameters (in Å) and volumes (in Å^3) of argyrodites Li_6PS_5X (X = Cl, I) and tetragonal α-Na_3PS_4 using different exchange and correlation functionals. The relative error of the predicted volumes concerning the experimental values is shown in percentage.

Functional	Lattice constants	Volume	ΔV/V %
	Li_6PS_5Cl		
Exp.[1]	9.898	969.711	—
PBE	10.005	1003.884	3.5
PBEsol	9.846	951.370	–1.9
SCAN	10.229	1070.162	10.3
R2SCAN	10.258	1079.566	10.2
SCAN+rvv10	10.193	1058.729	8.4
optB88	9.905	970.084	0.04
	Li_6PS_5I		
Exp.[1]	10.141	1043.007	—
PBE	10.199	1064.860	2.1
PBEsol	10.051	1024.023	–1.8
SCAN	10.152	1052.573	0.92
R2SCAN	10.173	1058.733	1.51
SCAN+rvv10	10.105	1039.942	–0.29
optB88	10.118	1044.546	0.15
	α-Na_3PS_4		
Exp.[2]	6.96, 7.09	343.745	—
PBE	6.98, 7.13	347.516	1.09
PBEsol	6.86, 6.99	329.235	–4.22
SCAN	6.85, 7.00	328.016	–4.58
R2SCAN	6.86, 7.01	330.209	–3.94
SCAN+rvv10	6.82, 6.95	323.209	–5.97
optB88	6.89, 7.03	333.324	–3.03

Sec. S3 Activation Energies

Table S6: Activation energies E_a (in eV) derived from Arrhenius plots with the estimated standard errors(stderr), and room temperature (300 K) conductivities σ_{RT} (in mS/cm), for Li_6PS_5Cl using MTPs trained with different strategies.

MTP type	Ea ± stderr	σ_{RT}	Experimental E_a	Experimental σ_{RT}
Exchange-correlation functional				
PBE	0.392 ± 0.002	0.145	0.45 ± 0.02[1]	∼0.01-4.96[1,3–6]
PBE-Exp lattice.	0.362 ± 0.006	0.260	–	–
PBEsol	0.421 ± 0.006	0.070	–	–
PBEsol-Exp lattice	0.368 ± 0.006	0.240	–	–
SCAN+rvv10	0.368 ±0.005	0.234	–	–
OptB88	0.367 ± 0.002	0.227	–	–
Temperature				
High Temperature	0.349 ± 0.0009	0.365	–	–
Simulation time				
Less Snapshots	0.386 ± 0.003	0.252	–	–

Table S7: Activation energies E_a (in eV) derived from Arrhenius plots with the estimated standard errors(stderr), and room temperature (300 K) conductivities σ_{RT} (in mS/cm), for Li_6PS_5I using MTPs trained with different strategies.

MTP type	Ea ± stderr	σ_{RT}	Experimental E_a	Experimental σ_{RT}
Exchange-correlation functional				
PBE	0.630 ± 0.011	3.029 x 10^{-5}	0.380 ± 0.025[1]	$\sim 10^{-3}$ - 10^{-4}[1]
PBEsol	0.536 ± 0.017	0.0006	–	–
SCAN+rvv10	0.584 ± 0.003	6.166 x 10^{-5}	–	–
OptB88	0.613 ± 0.010	3.008 x 10^{-5}	–	–
Temperature				
High Temperature	0.505 ± 0.016	0.001	–	–
Simulation time				
Less Snapshots	0.572 ± 0.027	0.0002	–	–

Table S8: Activation energies E_a (in eV) derived from Arrhenius plots with the estimated standard errors(stderr), and room temperature (300 K) conductivities σ_{RT} (in mS/cm), for Na_3PS_4 containing Na^+ vacancies (2%) using different types of MTPs.

MTP type	Ea ± stderr	σ_{RT}	Experimental E_a	Experimental σ_{RT}
Exchange-correlation functional				
PBE	0.057 ± 0.003	108.476	0.364 ± 0.015[7]	0.15 ± 0.01[7]
PBEsol	0.054 ± 0.002	106.991	–	–
R2SCAN	0.071 ± 0.002	64.536	–	–
OptB88	0.077 ± 0.005	52.686	–	–
AIMD-PBEsol	0.134 ± 0.007	26.539	–	–
de Klerk and Wagemaker[8]	0.160 ± 0.000	–	–	–
Temperature				
Low Temperature	0.054 ± 0.0008	108.978	–	–
Simulation time				
More Snapshots	0.063 ± 0.002	89.701	–	–

Table S9: Activation energies E_a (in eV) derived from Arrhenius plots with the estimated standard errors(stderr), and room temperature (300 K) conductivities σ_{RT} (in mS/cm) for Li_6PS_5Cl containing different types of defects, i.e., Li interstitials Li_i, antisites Cl_s and S_{Cl}, and Li^+ vacancies V_{Li^+}. Li_i are the intrinsic defect types. The exchange-correlation functional used is PBEsol. The MTPs used are trained specifically for each defect type. The defect concentrations for each type during MTP-MD simulations are taken from Gorai et al[9]

Defect	Ea ± stderr	σ_{RT}	Experimental E_a	Experimental σ_{RT}
$\mathrm{Li_i}$	0.421 ± 0.006	0.070	0.45 ± 0.02[1]	∼0.01-4.96[1,3–6]
$\mathrm{Cl_s}$	0.462 ± 0.008	0.041	–	–
$\mathrm{S_{Cl}}$	0.259 ± 0.011	0.492	–	–
$\mathrm{V_{Li}}$	0.411 ± 0.009	0.094	–	–

Table S10: Activation energies E_a (in eV) derived from Arrhenius plots with the estimated standard errors(stderr), and room temperature (300 K) conductivities σ_{RT} (in mS/cm) for $\mathbf{Li_6PS_5Cl}$ containing antisite Cl_s and V_{Li^+} at different concentrations (in cm^{-3}). The exchange-correlation functional used is PBEsol. The MTPs used are trained specifically for each defect type.

Defect Concentration	E_a		σ_{RT}	
	Cl_s	V_{Li^+}	Cl_s	V_{Li^+}
2.10 x 10^{21}	0.219 ± 0.012	0.277 ± 0.008	25.626	1.123
1.31 x 10^{20}	0.323 ± 0.018	0.419 ± 0.016	0.586	0.078
1.64 x 10^{19}	0.462 ± 0.008	0.411 ± 0.010	0.041	0.09
4.86 x 10^{18}	0.443 ± 0.005	0.419 ± 0.007	0.056	0.077
2.05 x 10^{18}	0.438 ± 0.011	0.443 ± 0.006	0.062	0.055
1.05 x 10^{18}	0.445 ± 0.002	0.441 ± 0.006	0.053	0.057

Table S11: Activation energies E_a (in eV) derived from Arrhenius plots with the estimated standard errors(stderr), and room temperature (300 K) conductivities σ_{RT} (in mS/cm) for $\mathbf{Li_6PS_5Cl}$ containing antisite Cl_s and V_{Li^+} at different concentrations (in cm^{-3}). The exchange-correlation functional used is PBEsol. The MTPs used are trained for Li_i.

Defect Concentration	E_a		σ_{RT}	
	Cl_s	V_{Li^+}	Cl_s	V_{Li^+}
5.24 x 10^{20}	0.258 ± 0.004	0.279 ± 0.011	10.228	1.055
1.31 x 10^{20}	0.366 ± 0.019	0.387 ± 0.014	0.230	0.118
1.64 x 10^{19}	0.390 ± 0.036	0.399 ± 0.013	0.116	0.101
4.86 x 10^{18}	0.386 ± 0.003	0.354 ± 0.018	0.142	0.266
2.05 x 10^{18}	0.400 ± 0.003	0.406 ± 0.008	0.111	0.100
1.05 x 10^{18}	0.398 ± 0.004	0.398 ± 0.002	0.115	0.114

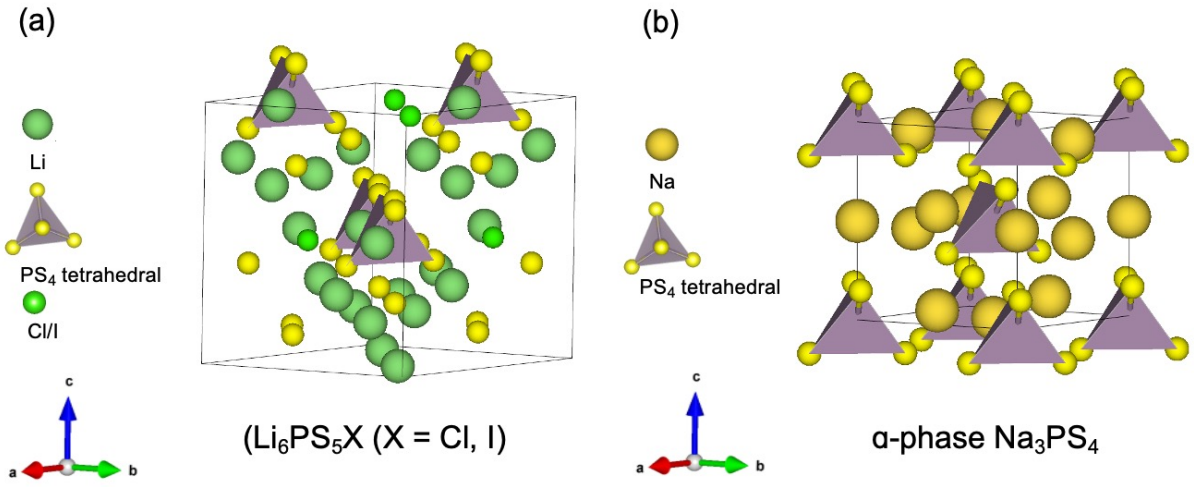

Figure S1: Crystal structures of (a) argyrodites Li_6PS_5X (X = Cl, I) and (b) tetragonal α-Na_3PS_4

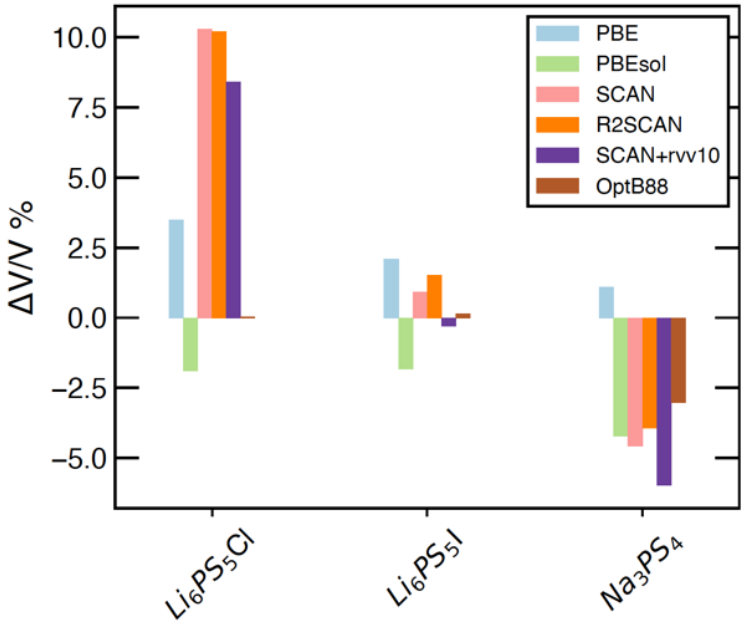

Figure S2: Comparison of the predicted volumes of argyrodites Li_6PS_5X (X = Cl, I) and Na_3PS_4 using different functionals. The relative error of the predicted volumes concerning experimental values is shown in percentage.

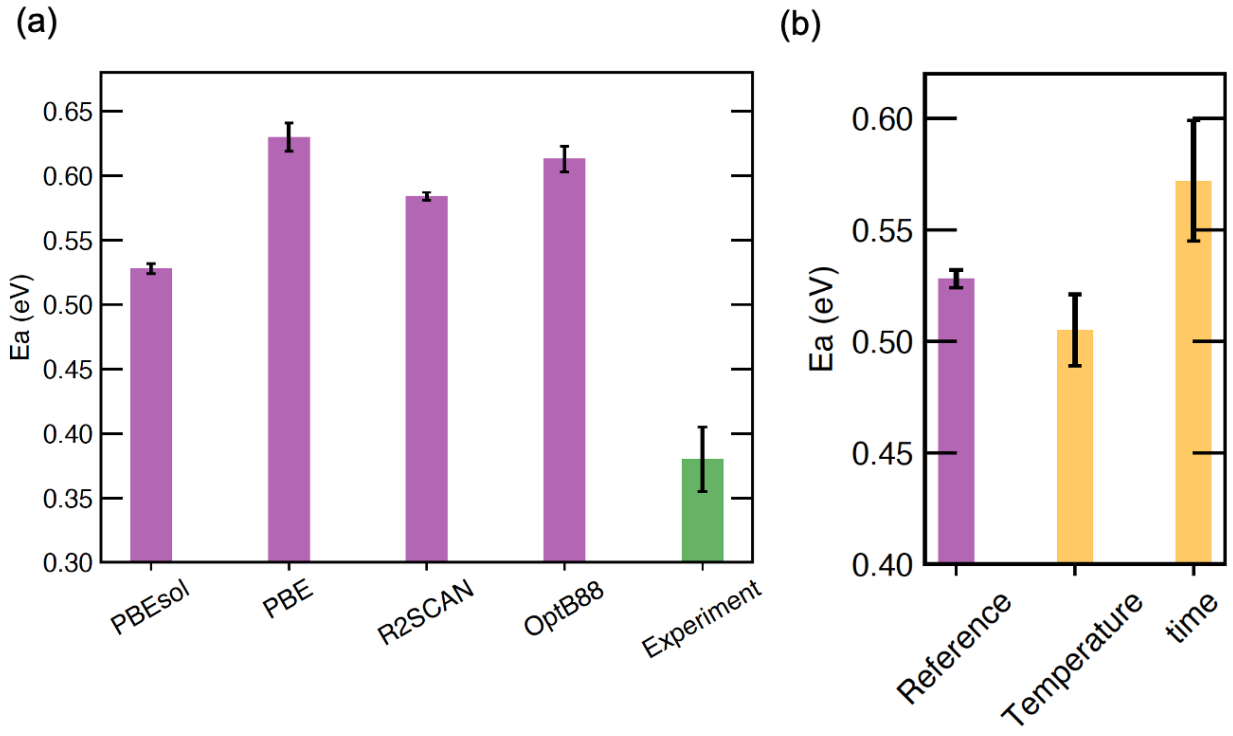

Figure S3: Activation energies E_a (in eV) derived from Arrhenius plots with the estimated standard errors(stderr) for Li_6PS_5I using MTPs trained with different strategies. (a) The computational variable considered is exchange-correlation functional. The experimental value is labeled in green, and (b) the computational variables considered are simulation temperature and time. The exchange-correlation functional is fixed to PBEsol. 'Reference' refers to the value of 'PBEsol' in (a).

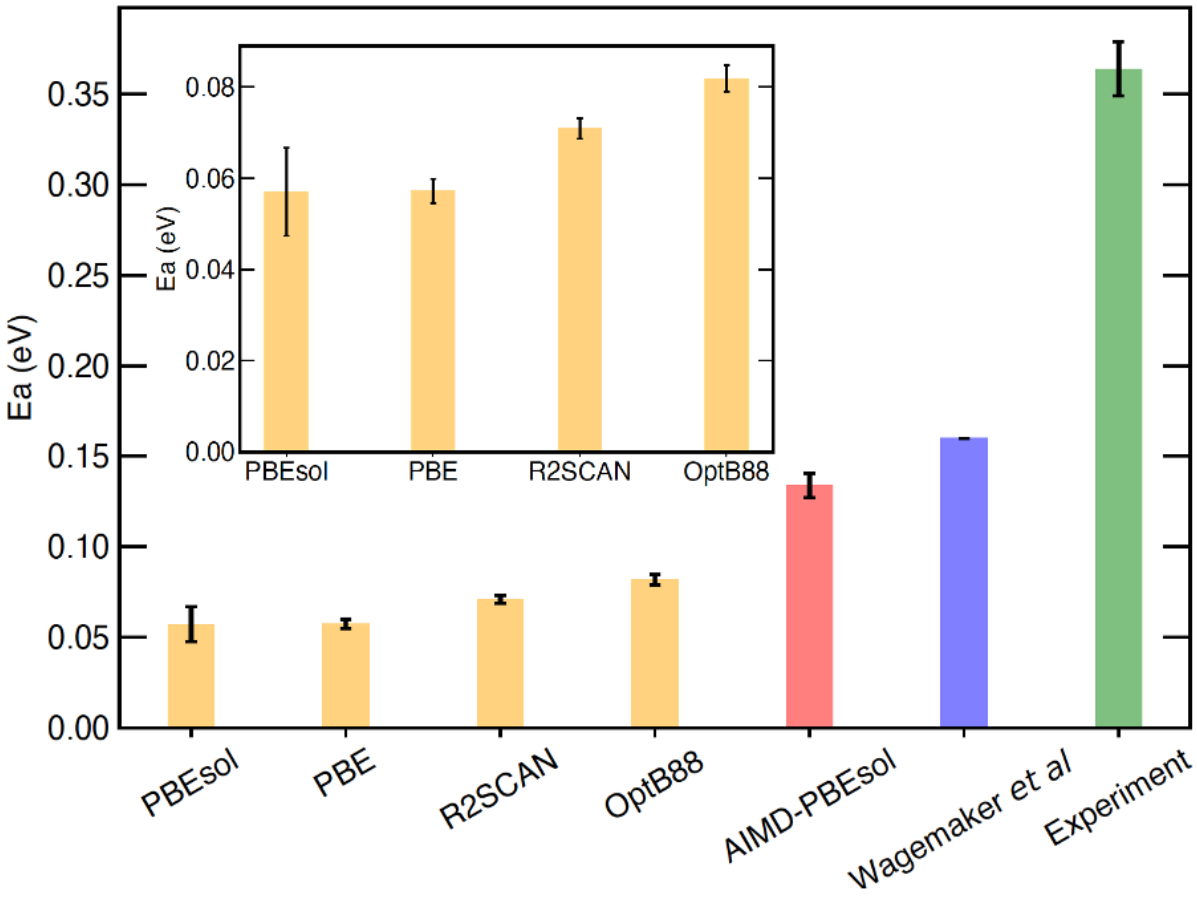

Figure S4: Activation energies (E_a) derived from Arrhenius plots with the estimated standard errors(stderr) for Na_3PS_4 using MTPs trained with different strategies. E_a calculated by using different functionals are shown in the zoom-in plot. E_a calculated by using the strategy 'Temperature' and 'Simulation time' are included in the error bar of the result for 'PBEsol'. E_a calculated by 40 ps-long AIMD simulations are labeled in red. E_a taken from de Klerk et al[8] is labelled in blue, where the error in E_a is not reported. The experimental value is labeled in green.[1]

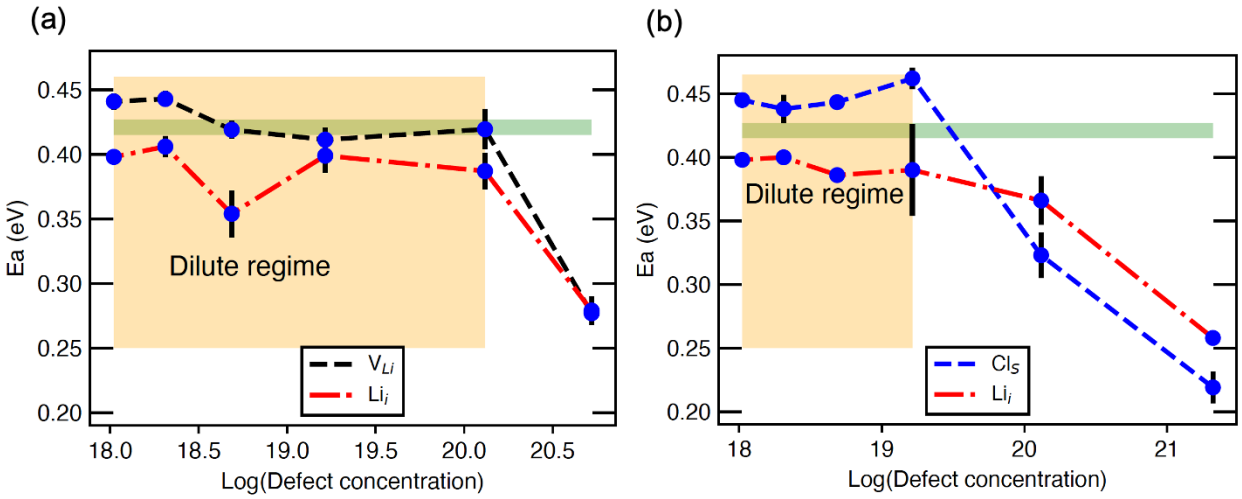

Figure S5: Activation energies (E_a) derived from Arrhenius plots with the estimated standard errors(stderr) for Li_6PS_5Cl containing (a) V_{Li} and (b) antisite Cl_S with different concentrations (in cm^{-3}). The exchange-correlation functional used is PBEsol. E_a of Li_i with error bars calculated from MTP@PBEsol are labeled in green, and the regions where E_a of either V_{Li} or Cl_S are close to the green region are labeled in yellow and considered as the dilute regimes. The MTPs used are either trained for Li interstitials (labeled as Li_i) or specifically for each defect type (labelled as V_{Li} and Cl_S, respectively).

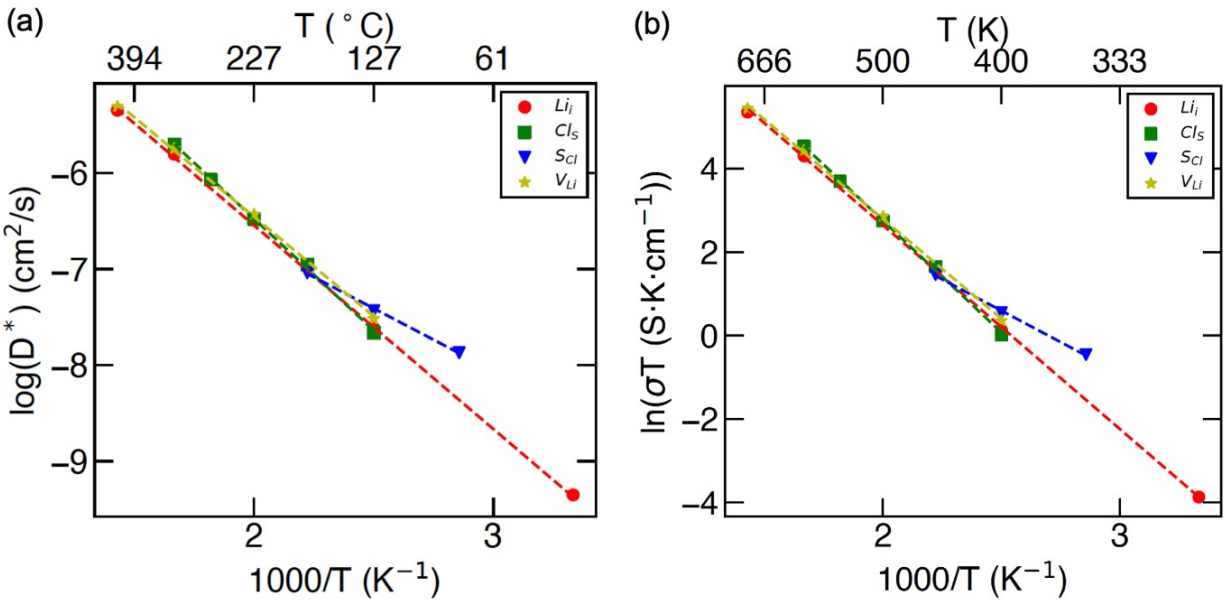

Figure S6: The calculated Li^+ transport properties of argyrodite Li_6PS_5Cl containing different types of defects, i.e., Li interstitials Li_i, antisites Cl_S and S_{Cl}, and Li^+ vacancies V_{Li}. Li_i are the intrinsic defect types. (a) Li^+ diffusivity (in cm^2/s) and (b) conductivity (in mS/cm). The exchange-correlation functional used is PBEsol. The MTPs used are trained specifically for each defect type. The defect concentrations for each type during MTP-MD simulations are taken from Gorai P et al.[9]

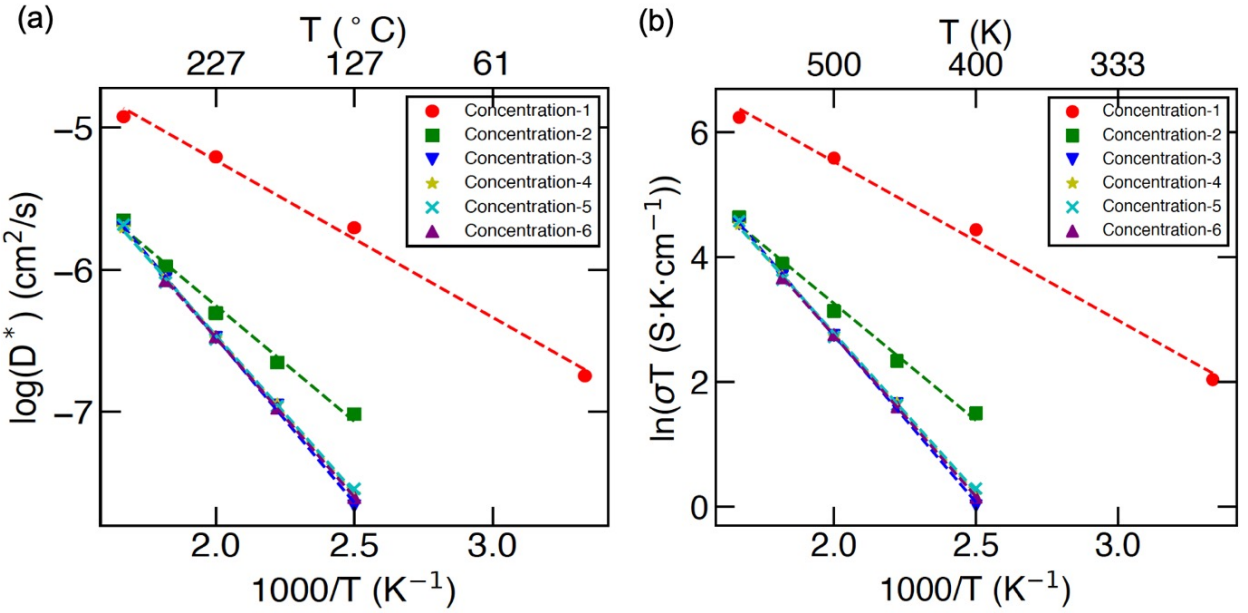

Figure S7: The calculated Li^+ transport properties of argyrodite Li_6PS_5Cl containing antisites Cl_S with different concentrations (in cm^{-3}). (a) Li^+ diffusivity (in cm^2/s) and (b) conductivity (in mS/cm). The exchange-correlation functional used is PBEsol. The MTPs used are trained for Cl_S

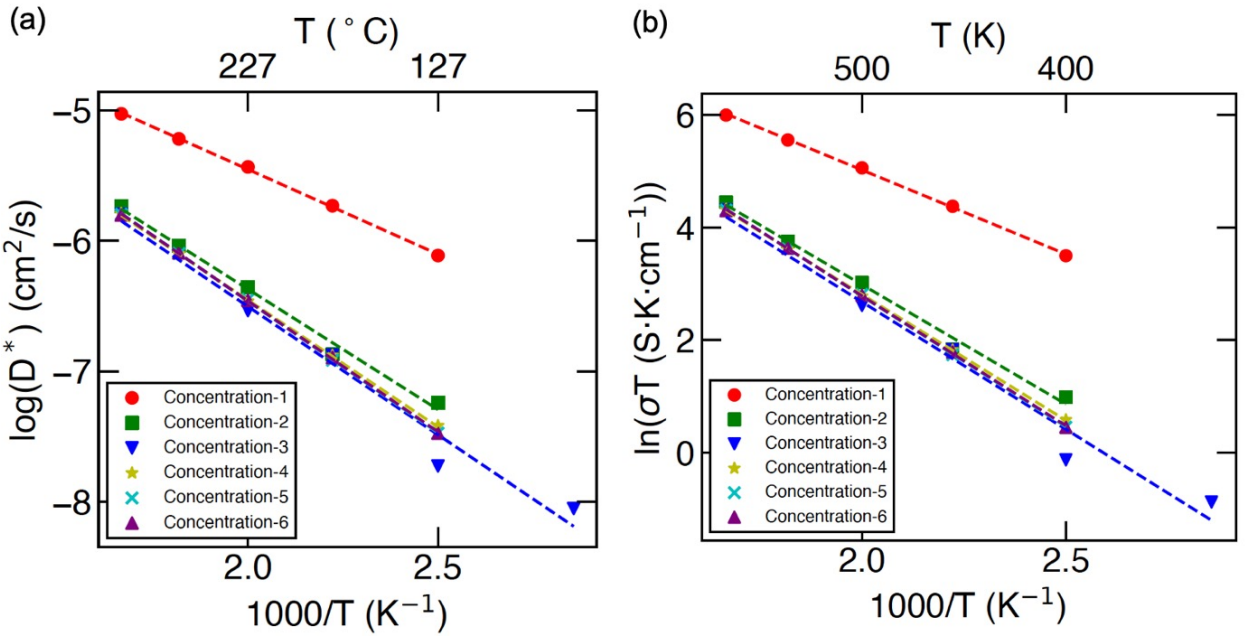

Figure S8: The calculated Li^+ transport properties of argyrodite Li_6PS_5Cl containing antisites Cl_S with different concentrations (in cm^{-3}). (a) Li^+ diffusivity (in cm^2/s) and (b) conductivity (in mS/cm). The exchange-correlation functional used is PBEsol. The MTP used is trained for Li_i

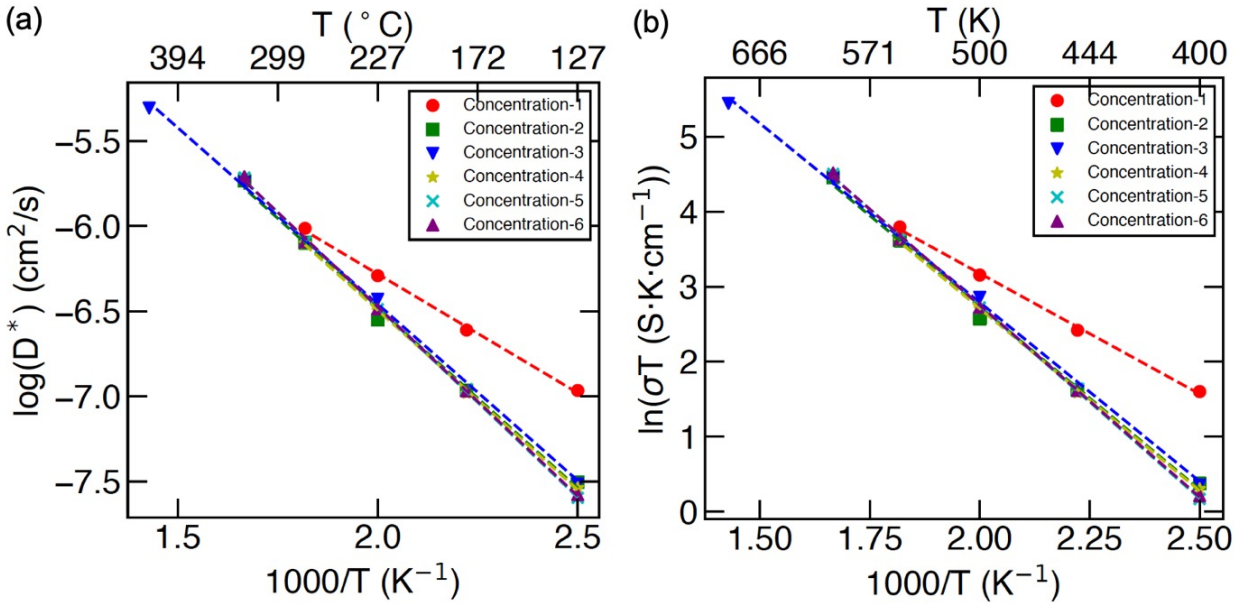

Figure S9: The calculated Li^+ transport properties of argyrodite Li_6PS_5Cl containing V_{Li} with different concentrations (in cm^{-3}). (a) Li^+ diffusivity (in cm^2/s) and (b) conductivity (in mS/cm). The exchange-correlation functional used is PBEsol. The MTP used is trained for V_{Li}

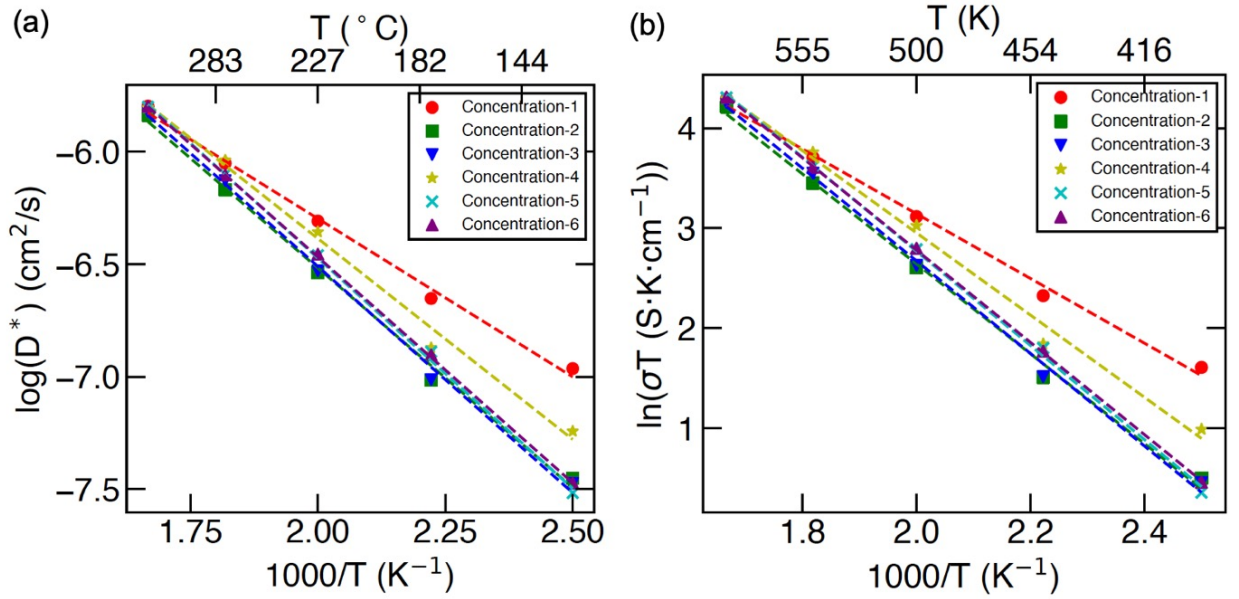

Figure S10: The calculated Li^+ transport properties of argyrodite Li_6PS_5Cl containing V_{Li} with different concentrations (in cm^{-3}). (a) Li^+ diffusivity (in cm^2/s) and (b) conductivity (in mS/cm). The exchange-correlation functional used is PBEsol. The MTP used is trained for Li_i

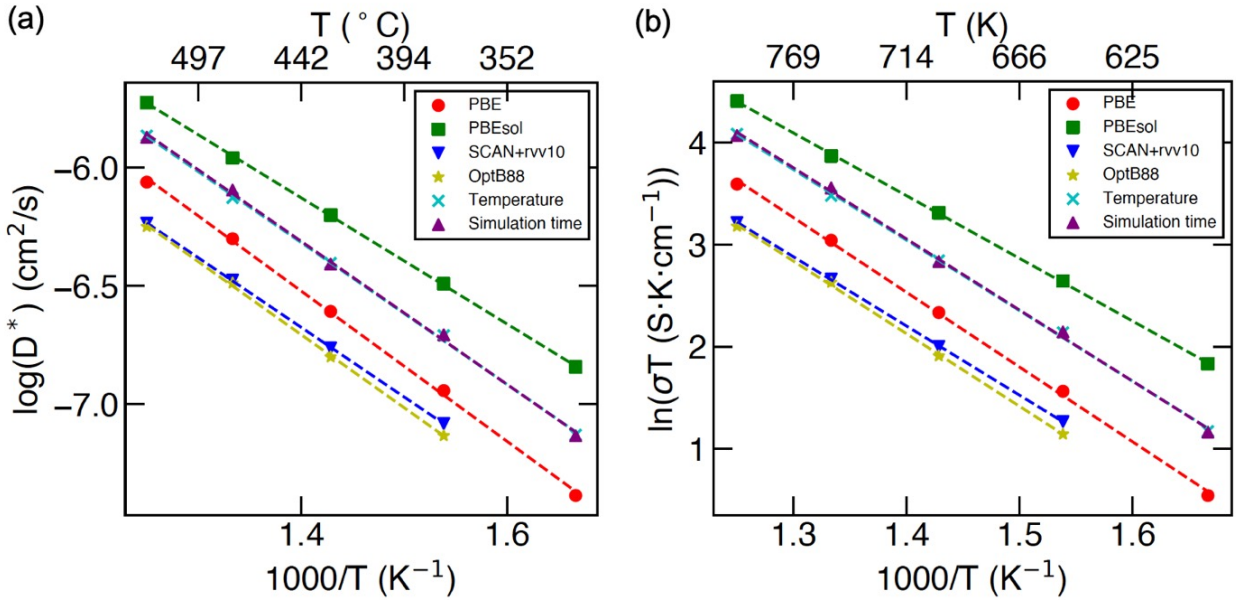

Figure S11: The calculated Li^+ transport properties of argyrodite Li_6PS_5I using different types of MTPs. (a) Li^+ diffusivity (in cm^2/s) and (b) conductivity (in mS/cm).

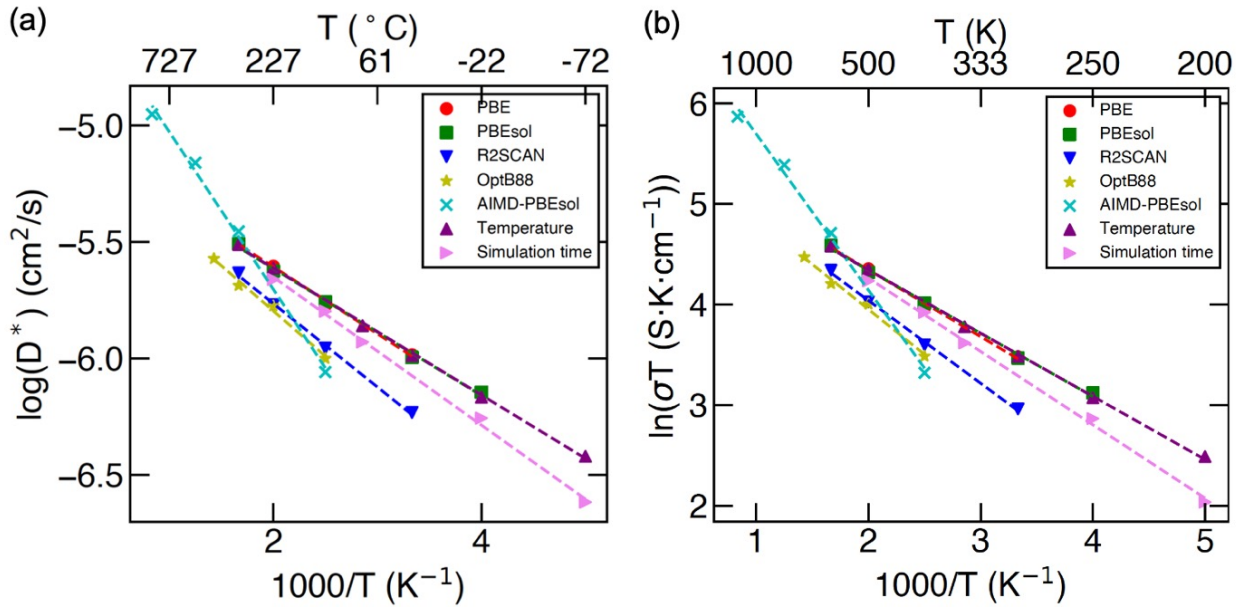

Figure S12: The calculated Na^+ transport properties of Na_3PS_4 by using MTPs trained with different strategies. (a) Na^+ diffusivity (in cm^2/s) and (b) conductivity (in mS/cm).

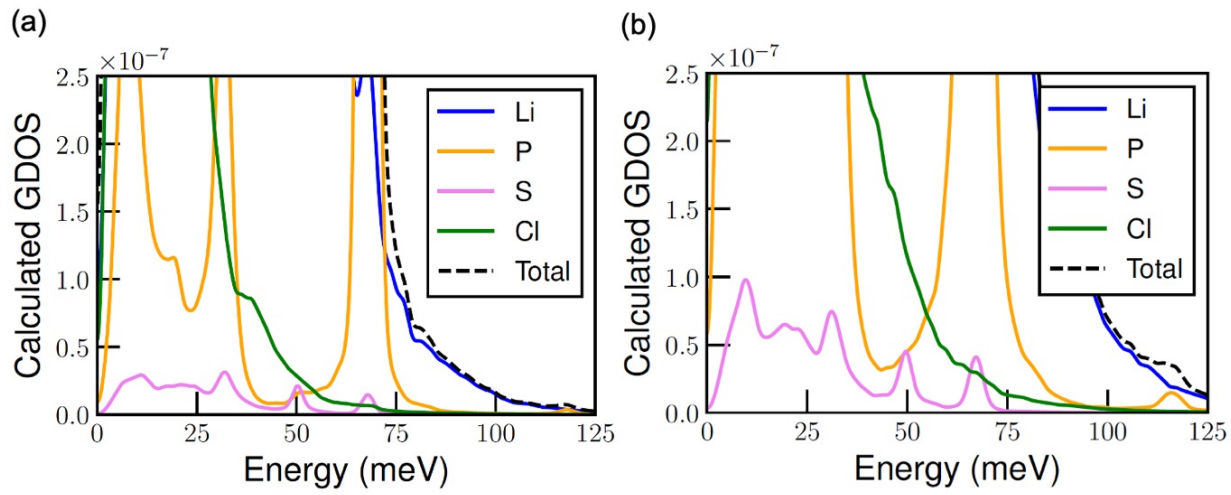

Figure S13: Zoom-in plots of generalized phonon density of states (GDOS) of Li atoms in argyrodites Li_6PS_5Cl calculated from MTP-MD simulations at (a) 300 K and (b) 500 K.

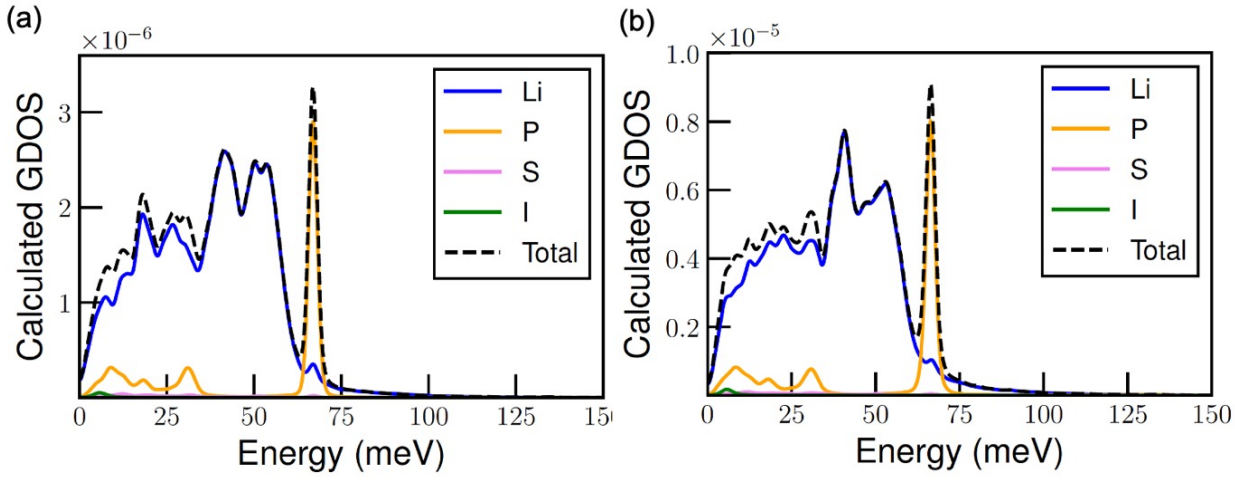

Figure S14: Generalized phonon density of states (GDOS) of Li atoms in argyrodites Li_6PS_5I calculated from MTP-MD simulations at (a) 300 K and (b) 500 K.

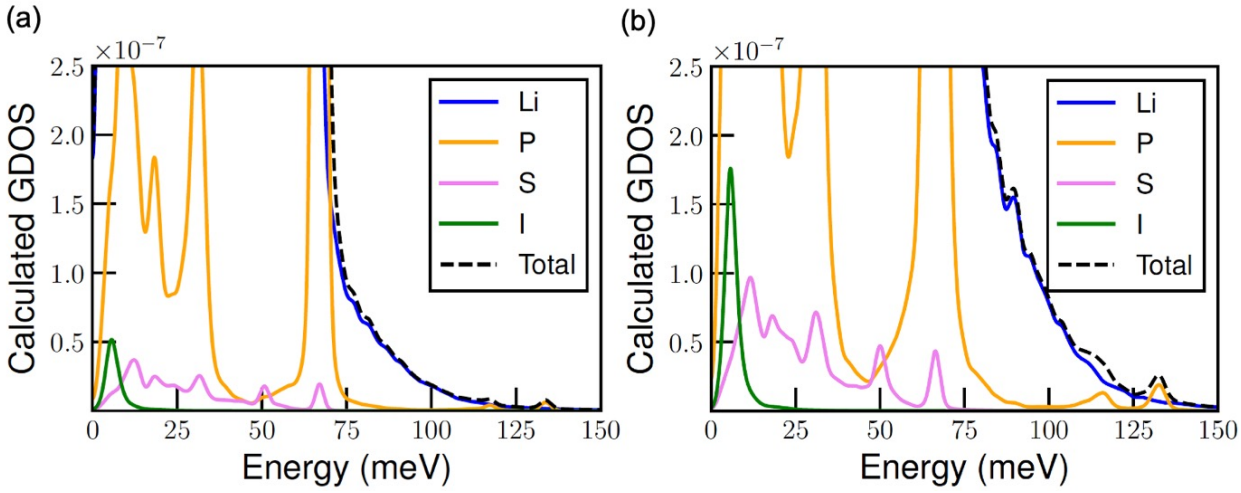

Figure S15: Zoom-in plots of generalized phonon density of states (GDOS) of Li atoms in argyrodites Li_6PS_5I calculated from MTP-MD simulations at (a) 300 K and (b) 500 K.

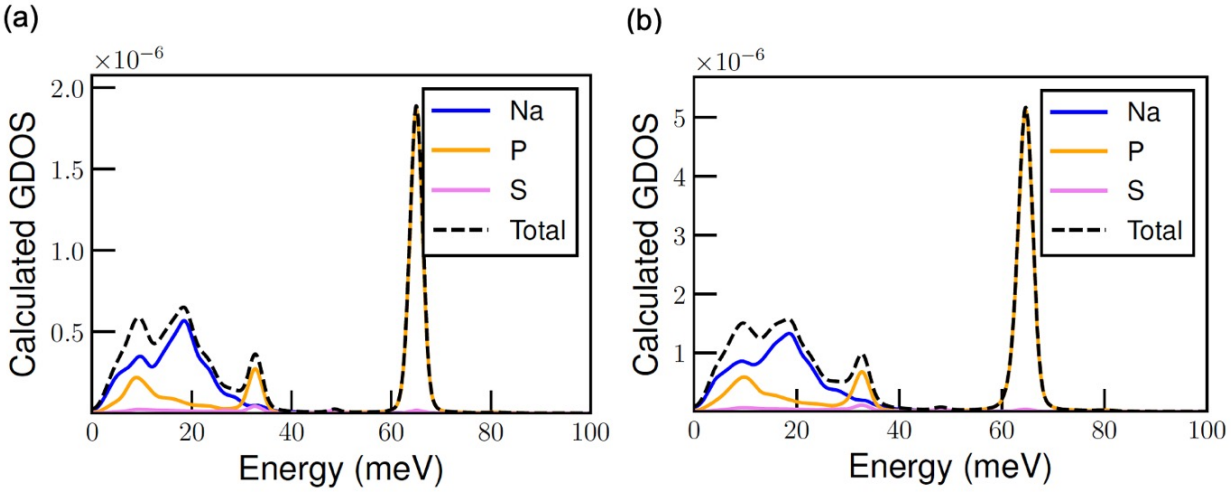

Figure S16: Generalized phonon density of states (GDOS) of Na atoms in Na_3PS_4 calculated from MTP-MD simulations at (a) 300 K and (b) 500 K.

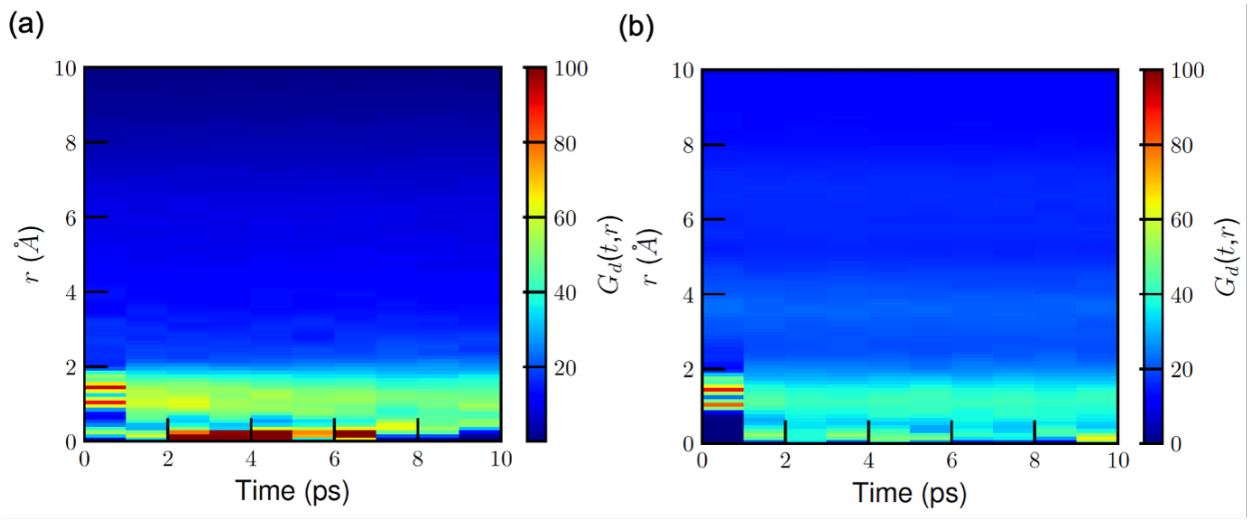

Figure S17: The distinct part of van Hove correlation function G_d calculated from MTP-MD simulations for (a) Li_6PS_5Cl and (b) Li_6PS_5I at 500K, at the initial 10 ps. The exchange-correlation functional used is PBEsol.

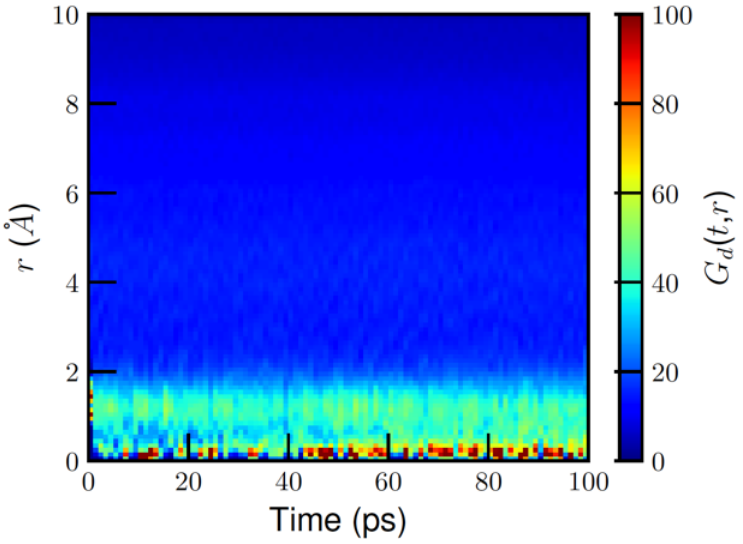

Figure S18: Distinct part of van Hove correlation function G_d calculated from MTP-MD simulations for Na_3PS_4. The exchange-correlation functional used is PBEsol.

References

(1) Kraft, M. A.; Culver, S. P.; Calderon, M.; Böcher, F.; Krauskopf, T.; Senyshyn, A.; Dietrich, C.; Zevalkink, A.; Janek, J.; Zeier, W. G. Influence of Lattice Polarizability on the Ionic Conductivity in the Lithium Superionic Argyrodites Li $_6$ PS $_5$ X (X = Cl, Br, I). *Journal of the American Chemical Society* **2017**, *139*, 10909–10918.

(2) Famprikis, T.; Bouyanfif, H.; Canepa, P.; Zbiri, M.; Dawson, J. A.; Suard, E.; Fauth, F.; Playford, H. Y.; Dambournet, D.; Borkiewicz, O. J.; Courty, M.; Clemens, O.; Chotard, J.-N.; Islam, M. S.; Masquelier, C. Insights into the Rich Polymorphism of the Na $^+$ Ion Conductor Na $_3$ PS $_4$ from the Perspective of Variable-Temperature Diffraction and Spectroscopy. *Chemistry of Materials* **2021**, *33*, 5652–5667.

(3) Rayavarapu, P. R.; Sharma, N.; Peterson, V. K.; Adams, S. Variation in Structure and Li+-Ion Migration in Argyrodite-Type Li6PS5X (X = Cl, Br, I) Solid Electrolytes. *Journal of Solid State Electrochemistry* **2012**, *16*, 1807–1813.

(4) Yu, C.; Ganapathy, S.; Hageman, J.; van Eijck, L.; van Eck, E. R. H.; Zhang, L.; Schwietert, T.; Basak, S.; Kelder, E. M.; Wagemaker, M. Facile Synthesis toward the Optimal Structure-Conductivity Characteristics of the Argyrodite Li $_6$ PS $_5$ Cl Solid-State Electrolyte. *ACS Applied Materials & Interfaces* **2018**, *10*, 33296–33306.

(5) Boulineau, S.; Courty, M.; Tarascon, J.-M.; Viallet, V. Mechanochemical Synthesis of Li-argyrodite Li6PS5X (X=Cl, Br, I) as Sulfur-Based Solid Electrolytes for All Solid State Batteries Application. *Solid State Ionics* **2012**, *221*, 1–5.

(6) Deiseroth, H.-J.; Kong, S.-T.; Eckert, H.; Vannahme, J.; Reiner, C.; Zaiß, T.; Schlosser, M. Li6PS5X: A Class of Crystalline Li-Rich Solids With an Unusually High Li+ Mobility. *Angewandte Chemie International Edition* **2008**, *47*, 755–758.

(7) Krauskopf, T.; Culver, S. P.; Zeier, W. G. Local Tetragonal Structure of the Cubic Superionic Conductor Na $_3$ PS $_4$. *Inorganic Chemistry* **2018**, *57*, 4739–4744.

(8) de Klerk, N. J. J.; Wagemaker, M. Diffusion Mechanism of the Sodium-Ion Solid Electrolyte Na $_3$ PS $_4$ and Potential Improvements of Halogen Doping. *Chemistry of Materials* **2016**, *28*, 3122–3130.

(9) Gorai, P.; Famprikis, T.; Singh, B.; Stevanović, V.; Canepa, P. Devil Is in the Defects: Electronic Conductivity in Solid Electrolytes. *Chemistry of Materials* **2021**, *33*, 7484–7498.